The impact of reach averaging Manning's equation for an in-situ dataset of water surface elevation, width, and slope

Stephen Tuozzolo[a,*], Theodore Langhorst[a], Renato Prata de Moraes Frasson[a], Tamlin Pavelsky[b], Michael Durand[a,c], Jessica J. Schobelock[d]

[a] Byrd Polar and Climate Research Center, The Ohio State University, 119 Scott Hall, 1090 Carmack Rd, Columbus, OH 43210, USA
[b] Department of Geological Sciences, University of North Carolina, Chapel Hill, NC, USA
[c] School of Earth Sciences, The Ohio State University, Columbus, OH, USA
[d] Virginia Polytechnic Institute and State University, Blacksburg, VA, USA

ARTICLE INFO

This manuscript was handled by Marco Borga, Editor-in-Chief, with the assistance of Francesco Comiti, Associate Editor.

Keywords:
River discharge
Manning's equation
Surface Water and Ocean Topography Mission

ABSTRACT

The Surface Water and Ocean Topography Mission (SWOT) will generate global, spatially continuous maps of water surface elevation and extent for large inland water bodies when it launches in 2021. We present an analysis of water surface elevation, width, and bathymetry timeseries data from a medium-sized (average annual discharge 14 m^3/s) river to explore Manning's equation, an empirical open channel flow equation, in the context of SWOT discharge algorithms. While this equation is in theory inapplicable to natural channels due to the non-uniform and spatially heterogeneous nature of river systems, we explored approaches to adapt it to this context using reach-averaged variables. At twenty sites along a 6.5 km stretch of the Olentangy River in Ohio, USA, we collected automated and manual measurements of water surface elevation and river width, undertook a full bathymetric survey of the study area, and built a hydraulic model. The stretch of river was divided into five reaches, and hydraulic variables were reach-averaged. Using these variables, we used a modified form of Manning's equation to compute a reach-averaged roughness coefficient. Reach-averaged roughness coefficients varied nonlinearly with discharge and were 2–10 times larger at low flow than at high flow in the in-situ data, ranging from 0.06 to 0.61 in one of the study reaches. These results were compared with the output of an unsteady flow simulation using a calibrated 1-D hydraulic model which was run with constant roughness coefficients at each cross section. When reach-averaged data was used, model-derived roughness coefficient also varied by more than an order of magnitude, with a range of 0.02–0.82 for one reach. For both in-situ and model-derived datasets, using a two-parameter roughness coefficient which scaled with a power law on either discharge or stage reduced discharge estimation error, with error for one reach dropping from 81% to 8% relative root-mean square error (rRMSE) in the in-situ data and 58% to 8% nRMSE in the modeled data. These results imply that spatial averaging of hydraulic variables leads to large variations in reach averaged Manning's n, which we term the reach's "effective resistance", and suggest that this variability can be accounted for with a simple parameterization in estimates of discharge that use spatially averaged data.

1. Introduction

Manning's equation and other empirical open-channel flow equations are convenient and commonly-used tools for hydrologists and engineers who seek to solve practical problems of channel design, flood wave modelling, and fluvial sediment transport (Dingman, 2009, p. 243). In research settings, applications of these equations include assessing flow in drainage canals (Froehlich, 2012) and indirectly estimating peak flood discharges (Asfaha et al., 2015; Lumbroso and Gaume, 2012). Although these equations are in principle considered by hydraulic textbooks to be inapplicable in non-uniform or unsteady flow (Sturm, 2001), they are also nonetheless regularly used to estimate discharge, energy dissipation, and other physical phenomena in natural fluvial environments (Bjerklie et al., 2018; Bjerklie et al., 2005; David et al., 2011; Ferguson et al., 2017; Powell, 2014; Yochum et al., 2012).

Gradually-varied flow regimes in natural river reaches pose a particular challenge to the application of these equations because the representative hydraulic parameters (e.g. cross-sectional area and top width) vary significantly in space. Representing irregular cross-sections with average channel variables in Manning's equation is problematic

* Corresponding author.
E-mail address: Tuozzolo.1@osu.edu (S. Tuozzolo).

https://doi.org/10.1016/j.jhydrol.2019.06.038
Received 1 July 2018; Received in revised form 1 April 2019; Accepted 14 June 2019
Available online 02 July 2019

due to the equation's non-linearity: evaluation of Manning's equation using reach average variables does not yield reach average discharge. This issue was highlighted by Li et al. (1992), who showed that averaging spatial variability within channel reaches results in a revised form of open-channel flow equations where the friction term (roughness coefficient or Darcy-Weisbach's *f*) is dependent upon the spatial variances of the hydraulic parameters. This finding highlights both a problem and way forward for application of these equations in rivers – while cross-sectional non-uniformities exert non-linear effects, they can be accounted for if the spatial variability of the channel morphology can be measured or estimated.

The emergence of high-precision remote sensing measurements of water surface elevations (WSE) and slope has revived interest in applications of these open channel flow equations on natural rivers (Bjerklie et al., 2018; Tourian et al., 2017). The forthcoming Surface Water and Ocean Topography (SWOT) mission (http://swot.jpl.nasa.gov/) promises high-accuracy measurements of water surfaces for large rivers when its data are averaged across multi-kilometer spatial domains, with target error standard deviations of 10 cm height and 1.7 cm/km slope for a reach with an average width of 100 m wide and a flow distance of 10 km (Biancamaria et al., 2016; Desai, 2018; Frasson et al., 2017). A number of proposed SWOT discharge algorithms leverage these high-accuracy and spatially averaged water surface observations in channel geometry-based flow laws to solve for unknown bathymetric and resistance variables with encouraging preliminary results (Durand et al., 2014; Gleason and Smith, 2014; Gleason et al., 2014; Hagemann et al., 2017). However, the inability of SWOT and other remote sensing tools to accurately resolve open-channel flow parameters at small spatial scales and the difficulty of parameterizing the spatial variability of these parameters highlights the challenge of applying these equations in natural settings.

We take an empirical approach to reconciling the spatial variability issue by testing a hypothesis – that the roughness variability described by Li et al. (1992) can be parameterized as a unique function of reach-averaged channel variables, in particular the hydraulic depth of flow. Such an approach simplifies a more complex roughness parameterization by trying to approximate within-reach variability as a function of SWOT-observable, reach-averaged variables. This assumes that within-reach variability can be broadly parameterized as a function of stage or discharge, and theorizes that the spatial variance in channel hydraulic variables reduces as the river approaches bank-full flow; this hypothesis is generally accepted for spatial variations in water surface slope (Dingman, 2009, p. 228), and may be more controversially applied to sub-reach variability in width and flow velocity (MacWilliams et al., 2006). We also expand on a finding by Durand et al. (2016), which motivated this work by highlighting averaging-induced roughness variability in a test dataset for SWOT discharge algorithms, by showing parallel behavior in in-situ and modeled data and by proposing an empirical approach to account for the observed variability. In this paper, we first present an in-situ dataset of spatially distributed water surface elevation, slope, and width data from an urban reach of the Olentangy River in Central Ohio, USA and provide a hydraulic characterization of the observed data. We then evaluate this data in the context of Manning's equation using a series of empirical roughness parameterizations, and compare results with those from a calibrated 1-d hydraulic model of the river reach.

2. Background

2.1. Spatial scales of river morphology

Natural rivers are characterized by a variable and dynamic channel morphology on relatively small spatial scales. Moody and Troutman (2002) showed that the integral length scale of channel morphology – or correlation length – scales linearly with width and varies from one to two mean channel widths on rivers ranging in mean annual discharge from 0.9 m^3/s to 11,800 m^3/s. Another study found the confluence-bifurcation length of braided rivers was regularly 4–5 river widths (Hundey and Ashmore, 2009), suggesting significant and consistent spatial variation over relatively short reaches.

Variation at these length scales poses a challenge for accurate estimates of discharge using canonical open-channel flow equations, which are meant for uniform reaches where channel shape and the cross-sectional area of flow do not change in the direction of flow. Using the numbers from Moody and Troutman (2002), a 100 m wide river would have a correlation length of 100–200 m, meaning measurements of channel morphology would be non-representative if averaged across any greater length scale. Wetted perimeter, cross-sectional area of flow, and depth measurements can be taken at cross sections, but slope measurements require measurements over some distance, *dx*, in the direction of flow, and slope accuracy decreases as *dx* gets smaller. As an example, if water surface or bathymetric elevations are calculated with an accuracy of ± 2 cm on a 100 m river reach, slope errors would be on the order of 28 cm/km. The issue of spatial averaging is pronounced in remote sensing approaches to estimate river discharge, as image measurements are, by nature, more spatially distributed than *in-situ* techniques.

2.2. Spatial scales in remote sensing of rivers

Techniques to estimate river discharge, characterize flow, and measure bathymetry using data from airborne and spaceborne instruments function on broader spatial scales than their in-situ counterparts. Reliable WSE estimates from nadir altimeters often require river widths of 1 km, and altimeter footprint radii are on the order of kilometers (Birkett et al., 2002; Papa et al., 2010). Similarly, remote sensing measurements of width may rely on broad spatial scales to extract a 'mean effective' or 'reach-averaged' width from water masks (Smith et al., 1996), though newer approaches and higher resolution water masks allow for width calculations at spatial scales nearer to 'cross sections' than reaches (Pavelsky and Smith, 2008). Interferometric methods which leverage spatially continuous WSE measurements and water extent masks have been used to generate reach-averaged widths and slopes, but required a spatial domain of 734 km to resolve slopes as low as 1–2 cm/km with height accuracies on the order of tens of cm to m (Alsdorf et al., 2000; Alsdorf et al., 2007; LeFavour and Alsdorf, 2005).

SWOT will provide a substantial improvement over existing remote sensing tools with its WSE, width, and slope measurement accuracy, but SWOT reach averaged data products over rivers must be averaged across 1 km^2 water surface areas to sufficiently remove random noise from the data and meet the mission's measurement accuracy targets for WSE, width, and slope (10 cm, 10% and 1.7 cm/km, respectively). For a 100 m wide river, this equates to averaging along 10 km reaches (Desai, 2018; Frasson et al., 2017). An airborne variant of the Ka-band Radar Interferometer (KaRIn) instrument onboard SWOT, AirSWOT, has been used to generate SWOT-like measurements prior to mission launch, and a study of AirSWOT on the Tanana River in Alaska showed average slope errors of 1 cm/km when data were averaged over 10 km reaches (Altenau et al., 2017). SWOT's capabilities present a unique opportunity to improve global estimates of river discharge, but retrieving accurate discharge estimates from SWOT's spatially-averaged water surface measurements will require alternative approaches to applying open-channel flow equations (Pavelsky et al., 2014).

2.3. Open channel flow

This paper focuses on using hydraulic variables measurable by remote sensing instruments in open channel flow equations, which are convenient simplifications of more complex hydraulic processes and are attractive due to their data requirements and modest computational costs. Manning's equation is traditionally written as:

$$Q = \frac{1}{n} A R^{2/3} S^{1/2}, \tag{1}$$

where Q is volumetric discharge, n is a non-dimensional roughness coefficient, R is the hydraulic radius, S is the energy or friction slope, and A is the cross sectional area of flow.

In flows characterized by a low-Froude condition (Fr < 0.3, discussed further in Section 3.2), when the diffusive wave approximation to the Saint-Venant shallow water equations is appropriate (Garambois and Monnier, 2015), we can estimate the friction slope as equivalent to the sum of the bed slope and the change in water depth, giving:

$$S = \frac{\partial Z}{\partial x} + \frac{\partial Y}{\partial x}, \tag{2}$$

where $\frac{\partial Z}{\partial x}$ is the bed slope and $\frac{\partial Y}{\partial x}$ is the downstream change in depth; this is functionally equivalent to the water surface slope. Using the diffusive approximation and rewriting Eq. (1) to substitute width for the wetted perimeter following Strelkoff and Clemmens (2000), we arrive at a form of Manning's equation that is convenient for SWOT purposes:

$$Q = \frac{1}{n} (A_0 + \delta A)^{5/3} W^{-2/3} S^{1/2}, \tag{3}$$

where A_0 represents the unobservable cross-sectional area of flow, δA represents a trapezoidal approximation of the observable changes in cross-sectional area of flow relative to A_0, and W and S are water surface width and slope, respectively. features SWOT-observable variables in δA, W, and S, leaving n and A_0 unknown. This form of Manning's equation has been used extensively in pre-SWOT algorithm development; to solve for unknowns in n and A_0, these Manning's-based algorithms invoke continuity and use Bayesian (Durand et al., 2014; Hagemann et al., 2017) or inverse (Garambois and Monnier, 2015) methods. The algorithm developed by Hagemann et al. (2017) is the most recent Manning's equation-based SWOT discharge algorithm; it uses an extensive dataset of channel data from the United States to generate prior values for unknown variables in open-channel flow equations and estimates model error in Manning's equation at ~25%. However, it holds Manning's n constant in both time and space. This assumption may contribute to some of the assumed error in the Manning's equation model: a study using multiple SWOT algorithms on a large dataset of hydraulic model outputs suggested that, for Manning's equation-based algorithms, the assumption in these algorithms of a temporally constant roughness coefficient, n, may be a significant contributor to algorithm error for certain test cases (Durand et al., 2016).

2.4. Variability in Manning's n

Manning's equation uses a single parameter, n, to represent the frictional nature of a given channel cross section, and hydraulic reference manuals provide roughness guides for channels based on their composition and morphology (Chow, 1959, p. 89-127) (Akan, 2011). A channel's reference roughness is meant to be constant for all within-bank flows; however, studies of flow in natural rivers have frequently found variability in Manning's n, often in the form of a nonlinear, inverse relationship between n and stage or discharge (De Doncker et al., 2009; Rouse, 1943; Wallis and Knight, 1984). Frictional effects in rivers have been known to scale with the relative submergence of roughness elements in the channel (Bathurst, 1985), and from a physical perspective this phenomenon can be explained by the "law-of-the-wall", which equates frictional retardation to boundary shear stresses induced by roughness at the bed surface (Cardoso et al., 1989). Going beyond the "law of the wall", Ferguson (2007) proposed a variable power equation on Darcy-Weisbach's f to allow for roughness variation as a function of the roughness length scale of the channel bottom, adding into consideration the physical effects of 'form drag', a pressure force generated by pressure gradients around large-scale roughness elements in the channel bed (Powell, 2014).

These physical explanations for n variability may mask additional non-physical errors associated with using open-channel flow equations in natural channels. Li et al. (1992) used an analytical assessment of the Darcy-Weisbach equation to show that the spatial variability of channel form induced nonlinear effects on Darcy-Weisbach's roughness parameter, f, and conceived an 'effective resistance', a terminology we borrow in this paper. Li et al. (1992) showed that this 'effective resistance' is larger than the cross-sectional roughness and is a function of the variances of the channel geometry. The issue of within-reach variability and its effects when averaging hydraulic variables has been explored more deeply in reach-scale hydraulic geometry studies (Harman et al., 2008; Navratil and Albert, 2010) but has not been sufficiently explored in the context of Manning's equation. Understanding and properly parameterizing these non-physical variations in n is important for applications of Manning's equation in natural river and tidal channels (Ferguson, 2010) and is particularly important due to the impending launch of SWOT and the rapid growth of other remote sensing tools in the hydrological sciences.

3. Methods

3.1. Study area & study period

The study was conducted on a 6.5 km stretch of the Olentangy River in Ohio, USA. The watershed, contributing to our study reach is approximately 1300 km^2 and is characterized by a mix of agricultural and suburban land uses. Discharge in the study area is regulated for flood control and water use by a large storage dam 20 km upstream of the upstream end of the study reach. The study reach runs adjacent to suburban neighborhoods and a major highway and is semi-channelized. There are two low-head dams located 5.5 km and 6.5 km downstream from the start of the study area which are not used to regulate flow but which create substantial backwater pools. The riverbed is largely composed of cobbles and pebbles in the steep, free-flowing upstream portion of our study reach and transitions to sand and silt in the backwater-affected, slower-flowing downstream portions.

We used USGS gage #03226800 for discharge data, which is located 4.4 km upstream of the upstream end of the study reach and which reports an annual average discharge of 15 m^3/s. The watershed area of the USGS gage is 30 km^2 smaller than the watershed defined by the upstream end of our study reach, which is then 50 km^2 smaller than the watershed defined by the end of the study reach. The study period used for this analysis lasted from 3 December 2014 to 17 December 2014, when all loggers were functioning and properly submerged. During this period, discharge at the USGS gage ranged from 0.6 m^3/s to 12.5 m^3/s, with a mean of 3.0 m^3/s; while the ten water-year (2008–2018) mean annual flow is 14.4 m^3/s (SD = 4.6 m^3/s), the median annual flow is 4.24 m^3/s and the range of observed discharges in this study spans the 5th to 70th percentiles of flow.

3.2. In-situ timeseries data

The in-situ portion of the study generated a timeseries of river elevations and surface widths using a combination of regular, automated water level measurements and sporadic, manual water surface width measurements. We chose twenty approximately evenly spaced sites for in-situ measurements; their locations are shown in Fig. 1. Limitations on river access and the need to measure just up- and downstream of low-head dams precluded even spacing. At each study site, we installed a Solinst level logger on the riverbed to record relative water depths at 5 min intervals. Level loggers were attached to cinder blocks, which were tipped sideways and placed on the riverbed to minimize possible movement along the riverbed. A Leica Viva GS15 RTK GPS rover was used to tie in relative water depth to water surface elevation (WSE). Across all logger records, we found 18 obvious and

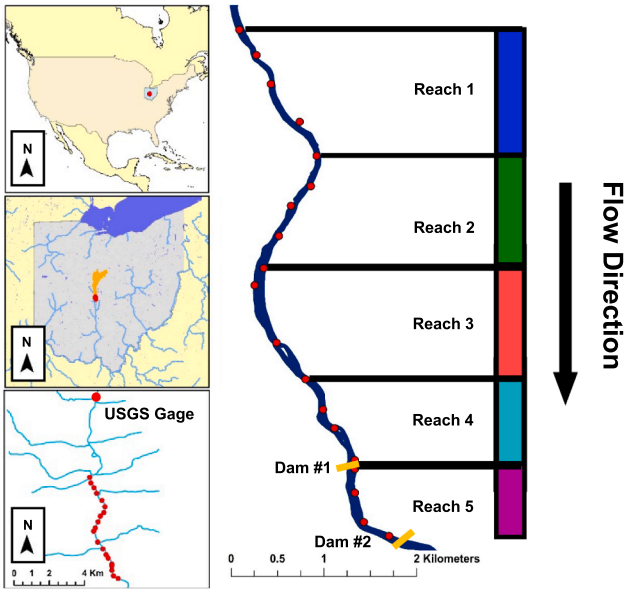

Fig. 1. Title: Map of study reach. The top left inset shows that watershed and state of Ohio in North America the top middle inset shows river centerlines and water bodies from U.S. Geological Survey (2000) and Pekel et al. (2016) in the state of Ohio, and the top right inset shows the study reach and tributaries, with the USGS gage upstream and yellow lines marking the low-head dams. (For interpretation of the references to colour in this figure legend, the reader is referred to the web version of this article.)

abrupt shifts in depth > 5 cm, which we corrected. Otherwise, we assumed that loggers did not move in the riverbed for the duration of the study. We converted logger-measured depths and GPS measurements to WSEs using a least-squares estimator which imposed a linear constraint on successive logger WSEs to force a downhill water surface profile at all sites and timesteps in the data, as described in Appendix A: Constrained logger elevation estimator. The accuracy and results of this estimator are presented in Section 4.1. We used a TruPulse laser rangefinder to measure the width of the river by measuring from shore to shore perpendicular to flow. Width measurements were taken during periods of both low and high flow to capture as much width variability as possible; this range of measurements allows for a full width-WSE relationship across the study period, which was then used to generate a continuous timeseries record of river widths for each site. Then, using a trapezoidal approximation of area, the change in cross sectional area δA was calculated using the following equation:

$$\delta A_i = \frac{w_i + w_0}{2}(h_i - h_0), \tag{4}$$

where w_i and h_i are the width and WSE at time i and h_0 is the initial WSE, when $\delta A_0 = 0$.

After finding WSE, width, and δA timeseries for each of the twenty sites, we averaged the data across reaches. The study area was split into five reaches after considering observable changes in the morphology, including the two low-head dams, and ensuring that each reach included at least four measurement sites. The five reaches had lengths of 979 m, 1449 m, 1543 m, 989 m, and 978 m. For each reach, a reach-averaged water surface slope timeseries, $\bar{S}$, was calculated by completing a first-order linear fit through the water surface elevation timeseries of all sites in the reach. In addition, reach-averaged timeseries values of WSE, width, and δA were calculated by taking the average of those values at all sites within a given reach at given time. Data shown in the results were averaged to hourly timesteps from the native five-minute measurement frequency to smooth out noise in the logger data; the analysis was also done at five-minute and fifteen-minute frequencies to match the native frequency of the logger and discharge data and showed nearly identical behavior, with the relative range of observed roughness changing by less than two percent between time-averaged and non-time averaged cases.

To compare with measured discharge at the USGS gage, we estimated the lag time between the gauge and the experimental reaches by looking at the rising limb of the high flow event as it traveled from the USGS gage to our study area and then past each pressure transducer. We used a constant celerity for the adjustment and were able to match discharge to the logger stage variations across the duration of the study period. Each reach then was assigned a time-shifted discharge from the USGS discharge data.

3.3. Bathymetric mapping of the study reach

After collecting WSE and width timeseries data, we conducted bathymetric measurements using boat-based and wading techniques. Measurements of water depth and water surface elevation from a kayak constituted the primary method of bathymetric data collection. The kayak was mounted with a Garmin GPSMAP 441s depth sounder to measure water depth and a Leica Viva GS15 RTK GPS to collect a reference water surface elevation. Geolocated depth measurements were transformed into river coordinates, which define each point by flow distance and distance perpendicular to river centerline (Legleiter and Kyriakidis, 2008). River coordinates were binned by flow distance to locations along the river centerline spaced 10–25 m apart, and the water surface elevation for each node was calculated as the median GPS elevation of data binned to that node, if there were at least 10 high quality GPS elevation measurements with a 3-d coordinate quality < 2 cm. A best-fit polynomial of those median centerline elevations was then used to estimate elevations for locations with insufficient elevation data. Due to the blanking distance of the depth sounder, the channel bottom was measured directly by wading with the Leica GPS in sections of the river less than 40 cm deep. In total, we collected over 33,000 bathymetric elevations from the kayak and manual GPS data. These elevation points were converted to an interpolated DEM of the river channel using a universal kriging method. We identified the channel edges using orthoimagery from the Ohio Geographically Referenced Information Project.

The bathymetric map of the study reach was used to calculate the cross-sectional area of flow at the beginning of the in-situ time series, A_0. WSEs from each logger were interpolated across reaches to 467 locations along the river centerline, and the difference between each bathymetry elevation pixel and the WSE for the closest interpolated river centerline point was taken as a depth. Those depths were multiplied by the pixel size of the bathymetry DEM raster (2.5 m × 2.5 m), and the total estimated volume of each reach was divided by the flow distance of each reach.

3.4. Hydraulic model development

After building the bathymetric map of the study area, a hydraulic model was developed by sampling the bathymetry at 115 cross sections; a portion of the interpolated bathymetry and cross sections for Reach 3 are shown in Fig. 2. The two low-head dams in the study area were included in the model by approximating the dam geometry using a previous study of the Olentangy River (Ringley, 2006). An unsteady simulation of the flow timeseries captured by the in-situ data from 3 December 2014 to 17 December 2014 was then run in the Hydrologic Engineering Centers River Analysis System (HEC-RAS). Boundary conditions were set by USGS discharge data from the in-situ study period along with elevations from our level logger at the downstream end of the field site. The unsteady flow simulation was run with a time step of 15 s to satisfy the Courant Condition. Manning's n was set to a constant value of 0.04 at every cross section following the previous study of the river reach. Flow remained inside the channel and did not increase to submerge bank-side vegetation or a substantially different substrate, so

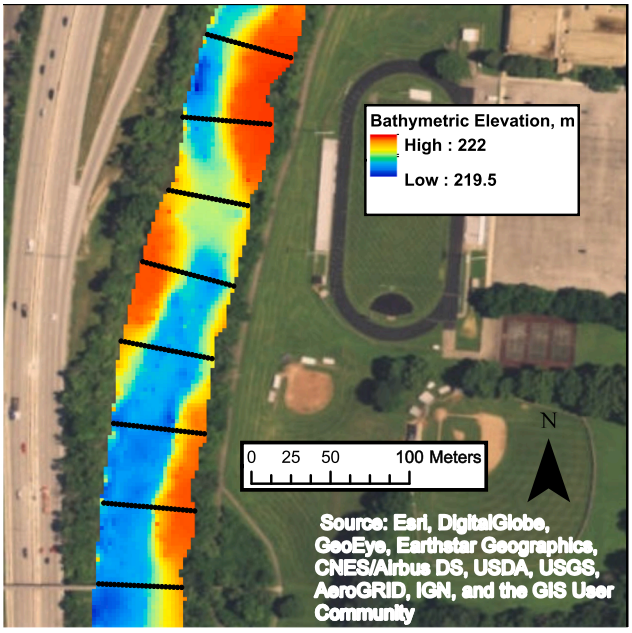

Fig. 2. Title: Example plan view of interpolated bathymetry with HEC-RAS cross sections.

we did not assign a variable roughness in the model.

After the simulation was run, data were averaged to hourly at each of the 115 cross sections, and cross-sectional timeseries data were grouped into the same reaches as the in-situ data for averaging using the same techniques: we used a geometric average to calculate mean cross-sectional area, water surface width, and discharge, and calculated water surface slope using a first order linear approximation slope using all water surface elevation measurements within the reach. This created a reach-averaged dataset of hourly area, width, water surface slope, and discharge for the five reaches. In addition to those data, the HEC-RAS model provides the friction slope used in Manning's equation, S_f, the hydraulic radius, R, and average velocity, V.

3.5. Hydraulic characterization

To justify using the water surface slope in Manning's equation, which requires a low Froude approximation, we characterized the hydraulic characteristics of the observed flow. Following the approach of Trigg et al. (2009), who used previous studies of appropriate approximations to the Saint-Venant equations (Moussa and Bocquillon, 1996; Vieira, 1983) to characterize the Amazon river floodwave across multiple broad river reaches, we calculated the Froude number, kinematic wave number, and wave period from the collected data using Eqs. (5)–(7), respectively.

$$F_0 = \frac{V}{(gy)^{0.5}}, \tag{5}$$

$$k = \frac{S_0 L}{y F_0^2}, \tag{6}$$

$$T+ = \frac{T V_0 S_{f0}}{y_0}, \tag{7}$$

In Eq. (5), F_0 is the Froude number V is the flow velocity; y is the depth of flow, and g is gravitational acceleration. In Eq. (6), k is the kinematic flow number, S_0 is the bed slope, and L is the reach length. In Eq. (7), $T+$ is the non-dimensionalized floodwave period, T is the floodwave period (approximated as the duration of the floodwave from baseflow to baseflow), and V_0 and S_{f0} are the water velocity and mean friction slope (approximated as the water surface slope) of the unperturbed, or non-flood, condition.

3.6. Effective resistance and fit to Manning's equation

Effective resistance, $\tilde{n}$, was directly calculated from 3 using reach-averaged values, as all values other than n are included in our time-series dataset. This allows us to solve for $\tilde{n}$ at each reach and time step in the dataset. After computing $\tilde{n}$ directly, we used a nonlinear least square tool to fit parameters to $\tilde{n}$ and assess different formulations of Manning's equation. We used four formulations of $\tilde{n}$ to evaluate their accuracy at parameterizing the effective resistance and minimizing difference between estimated $\tilde{n}$ values and those predicted by each formulation.

1. Assume resistance is a constant value, per Manning's equation, and estimate n:

$$\tilde{n} = \bar{n}, \tag{8}$$

2. Assume a power law relationship between resistance and the river stage, relative to the lowest observed flow variation. This requires estimating a and b:

$$\tilde{n} = a(H_t - H_0 + \delta H)^b, \tag{9}$$

In this equation, H_t is the river stage at time t, H_0 is the lowest observed river stage and δH is some small number (here equal to 0.1) to ensure the power law returns a nonzero number.

3. Assume a power law relationship between resistance and discharge; this again requires estimating parameters a and b:

$$\tilde{n} = aQ^b, \tag{10}$$

This relationship between ñ and Q can be further rearranged to show that if is correct then exponents for A, W, and S in Manning's equation must be modified; this algebraic rearrangement is shown in Appendix B.

4. Assume a logarithmic relationship between resistance and the depth of flow relative to bankfull flow; this assumption requires estimating n_b:

$$\tilde{n} = n^b\left(1 + \log\left(\frac{H - B}{h - B}\right)\right), \tag{11}$$

with n_b equal to the bank-full (reference) Manning n, H equal to bank-full (reference) stage, h equal to the stage at time of observation, and B equal to the stage at which $Q = 0$ (Bjerklie et al., 2018). This approach allows $\tilde{n}$ to approach n_b as the discharge approaches bankfull flow, but also requires knowledge of the stage at zero flow, or the average bathymetric elevation.

4. Results

4.1. In-situ measurements

After adjusting water surface elevations using the constrained least-squares estimator, we calculated error using a jackknife validation strategy and found a water surface elevation RMSE of 3.73 cm and a positive bias of 0.30 cm relative to 67 GPS measurements; the height validation points are shown in Fig. 3. Width-WSE relationships were established for each site using a linear regression and are displayed in Fig. 4 for all 20 sites; these relationships were used to calculate width timeseries for each site, and we set a requirement for a positive width-WSE relationship at $p < 0.05$. For the 6/20 sites which did not meet this requirement, we used the average width as a constant time-varying width. Fit statistics for all width regressions are given in Appendix C. We observe a high degree of within-reach variability in the width-

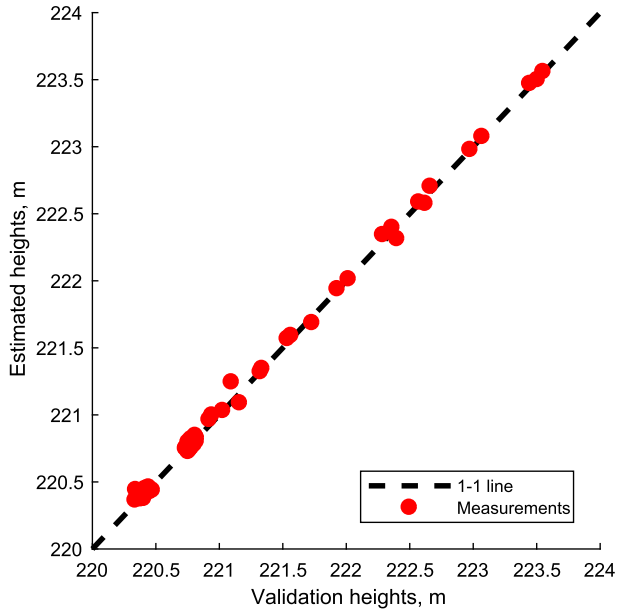

Fig. 3. Title: Elevations from constrained least squares estimator compared with independent GPS measurements. Caption: Estimator RMSE was 3.73 cm and bias was 0.30 cm.

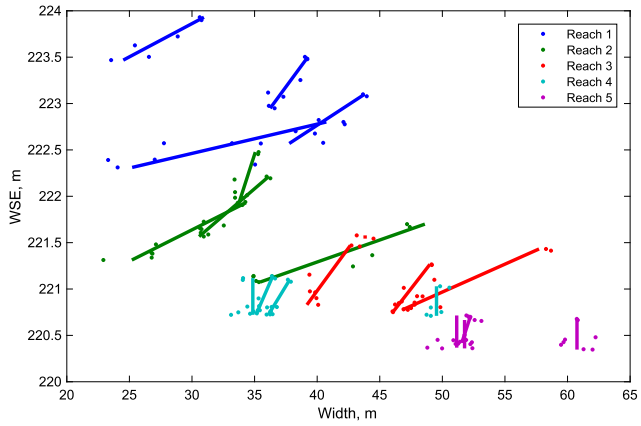

Fig. 4. Title: Width – Height measurements and a linear regression for all logger twenty sites. Caption: Width-height variation was larger in the upstream, high-gradient reaches (Reaches 1, 2, and 3), and small in the reaches adjacent to low-head dams (Reaches 4 and 5). The p and R^2 values of the linear fit, along with the slope of the height-width fit for sites with $p < 0.05$, is given in Appendix C: Fit statistics for all height-width rating curves.

height relationships, and see that width variation for the observed discharge range is highest in the steep, upstream reaches and lowest in the low-gradient, downstream reaches.

Reach-averaged cross-sectional area of flow, the sum of A_0 and δA as written in Eq. (3) and Eq. (4), ranged from 7 to 31 m^2 at Reach 2 to 70–89 m^2 at Reach 5, where widths were mostly invariant and areal variation was largely driven by stage variability. Fig. 5 shows the reach-averaged timeseries values of relative stage, slope, width, and cross-sectional area of flow. The relative stages of the five reaches alongside USGS gage data shows that the rising limbs of the hydrograph differ, with a dual peak of stage in the study area's discharge that is not apparent in the USGS gage station. This difference suggests that localized rainfall led to lateral inflows along the river between the USGS gage and our study area, a problem which likely added to our error when analyzing the data in the context of Manning's equation. We assume that Q is both constant within a given reach and constant between reaches after adjusting for flood wave celerity.

4.2. Observed hydraulics: in-situ and modeled data

For the steeper, upstream portion of the study area, in-situ water surface slopes (Fig. 5b) had maxima during the lowest recorded discharge and minima during the highest recorded discharge, varying from 143 cm/km to 132 cm/km and 76 cm/km to 63 cm/km in Reaches 1 & 2, respectively. For Reaches 3, 4, and 5, which are affected by the backwaters created by the two low-head dams at low-flow, the water surface slope increased dramatically with increased discharge, from 6 cm/km to 29 cm/km, 1 cm/km to 12 cm/km, and 2 cm/km to 7 cm/km for reaches 3, 4, and 5, respectively. The backwater 'pool' from the dam below Reach 4 moved upstream, creating a broader concave slope as shown in Fig. 6 for high and low flows.

As is seen in Fig. 6, the results of the unsteady flow simulation showed similar dynamics and variability in water surface slopes; overall, the WSE root mean square error was 13 cm across all reaches and time steps when compared with the in-situ data. The model and bathymetry data show that the water surface slope mostly follows the bed slope in the upstream reaches, but the effect of the first low-head dam leads to a deviation from the bed slope for 2 km upstream of the dam. Similar to the in-situ data, the upstream reaches were characterized by decreased slopes at high flow, while lower-gradient reaches featured increased slopes at high flow as the backwater 'pool' created by the low-head dams propagated upstream.

In Table 1, values for Eqs. (5), (6), and (7) are given at the lowest average, and highest recorded flow for all reaches. In Table 2, values for F_0, k, and $T+$ are given for all reaches for those same flows. The in-situ data is characterized by low Froude (F_0) numbers at all stages of observed flow, suggesting that the inertial term in the Saint-Venant equations is likely unimportant to the flow regime.

4.3. Effective resistance

Using known cross-sectional area of flow, water surface width, water surface slope, and discharge for each reach, the effective resistance, $\tilde{n}$, was calculated from both the in-situ and modeled data using Eq. (3). For in-situ data, which can be seen in the left panel of Fig. 7, $\tilde{n}$ varied with discharge in a non-linear way; high-flow effective $\tilde{n}$ was 0.09 at Reach 1 and 0.06 at Reach 5, while low-flow effective $\tilde{n}$ was 0.71 and 0.61 for the same reaches. The range in $\tilde{n}$ was largest at Reaches 1 and 5, where low-flow $\tilde{n}$ was 8 and 10 times larger than high-flow $\tilde{n}$, respectively. Variation was smallest at Reach 2, where low-flow $\tilde{n}$ was only 2.7 times larger than high-flow $\tilde{n}$. For modeled data, $\tilde{n}$ was calculated using A_{bar}, W_{bar}, S_{bar}, and a reach-centered Q. Reach-averaged values of A, W, and S created a similar variability to that observed in the in-situ data, with high-flow $\tilde{n}$ ranging from 0.08 at Reach 1 to 0.02 at Reach 5 and low-flow $\tilde{n}$ of 0.46 and 0.82 for the same reaches, despite the fact that the model was run with n = 0.04 and allowed for no expansion or contraction losses. In addition to the analysis using the water surface slope from the model, we observed similar $\tilde{n}$ variability and error patterns in the modeled data using the reach-averaged HEC-RAS 'friction slope', but only show the water surface slope results from the model to allow for a simple and direct comparison with the in-situ data.

4.4. Calibration of Manning's equation

The results of the least squares optimizations of Manning's equation (Eq. (4), with Eqs. (8–11) substituted for n) are given in Fig. 8 and Fig. 9. Fig. 8 shows the estimated $\tilde{n}$ for the optimized Manning's results for the in-situ and model output data. Eqs. (9) and (10) allow for a highly variable effective resistance which decreases with increasing stage and discharge, while Eq. (11) generates a similar but less pronounced variation in $\tilde{n}$. Fig. 9 shows the errors in estimating discharge after using the optimized parameters in Manning's equation, and Fig. 10 shows discharge estimates using the best-performing parameterization,

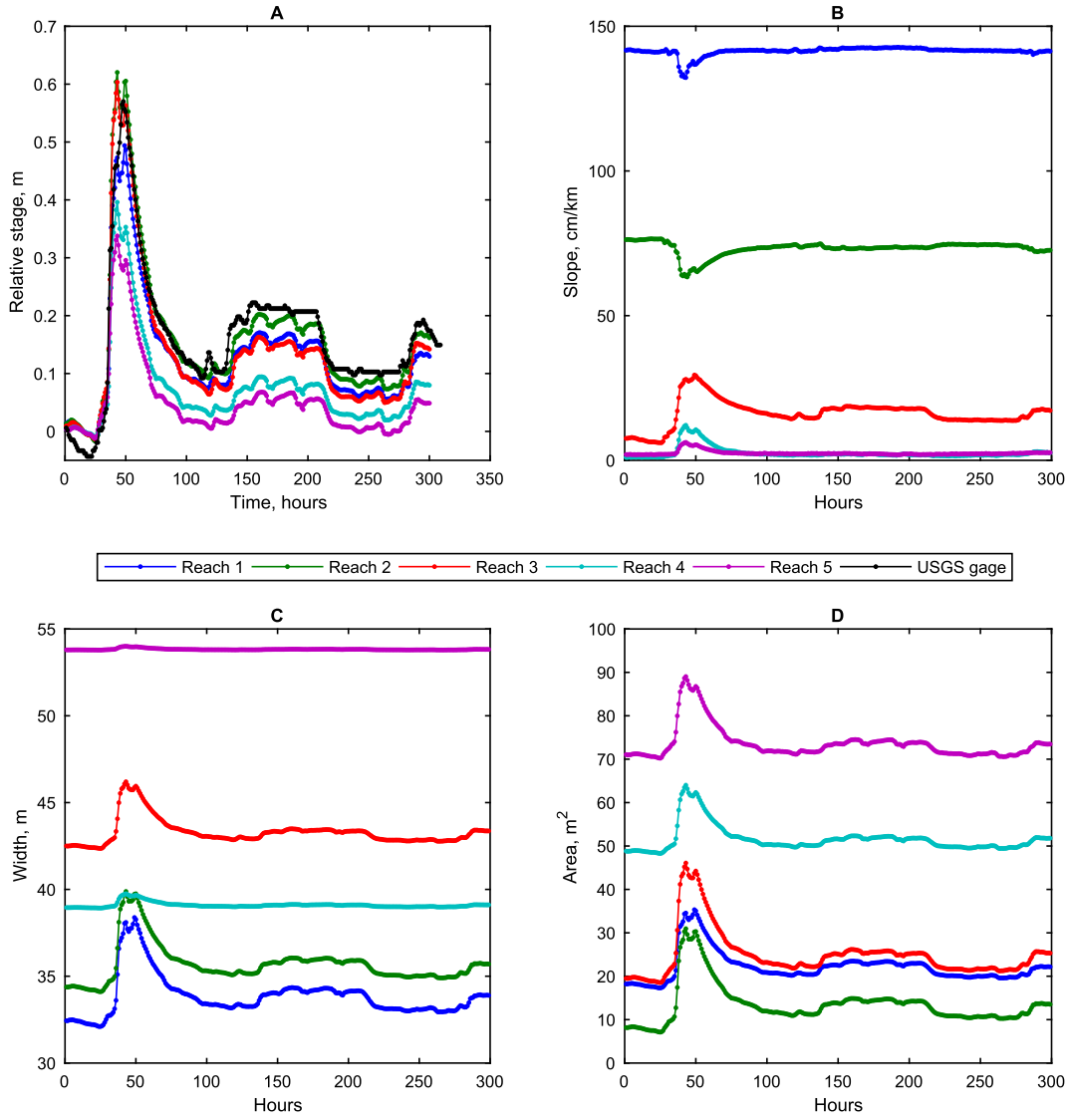

Fig. 5. Title: Reach-averaged values of stage (A), slope (B), width (C), and cross-sectional area of flow (D) for the study period. Caption: Note that the independent and dependent axes are switched, and that cross-sectional area of flow change is stage-driven in reaches where weak width-height correlations were found (e.g. Reach 5), but both width- and stage-driven in reaches where the width-height relationship was more apparent (e.g. Reach 1).

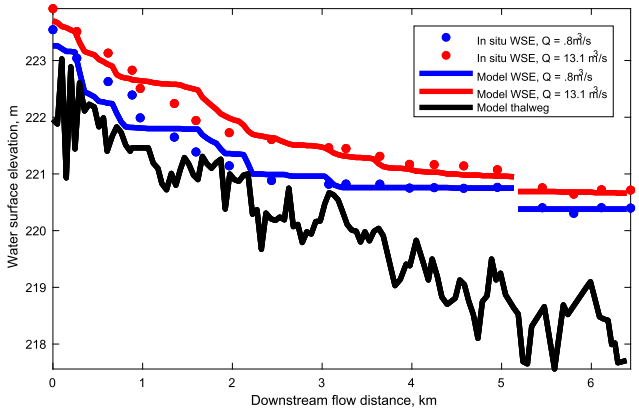

Fig. 6. Title: Water surface profile at low and high flow, and thalweg elevations from the HEC-RAS model.

Eq. (10). For the entire in-situ dataset timeseries, relative root mean square error (rRMSE) fell from an average of 61% for constant $\tilde{n}$ to 14%, 29%, and 50% for discharge-$\tilde{n}$ power law, stage-$\tilde{n}$ power law, and stage-$\tilde{n}$ logarithmic formulations. In the modeled data, similar patterns in error were observed, with errors reducing from 54% to 18%, 23%, and 40% for the same parameterizations when HEC-RAS generated water surface slope was used in Manning's equation. In both the modeled and in-situ data, these reductions in error were unevenly distributed across reaches. For example, for Reach 1, rRMSE of the in-situ data fit dropped from 81% using a constant $\tilde{n}$ to 8% using Eq. (9) and 15% using Eq. (10), while in the modeled data the rRMSE dropped from

Table 1
Flow depth, velocity, water surface slope for reaches 1–5. Data are provided for mean study period discharge, Q = 3 m^3/s (min discharge Q = 0.8 m^3/s, max discharge Q = 13 m^3/s).

Reach	Average depth, m	Average velocity, m/s	Surface Slope, cm/km	Reach length, m
1	0.67 (0.55, 0.92)	0.13 (0.04, 0.37)	12 (141, 137)	979
2	0.41 (0.21, 0.76)	0.20 (0.08, 0.44)	73 (77, 66)	1449
3	0.60 (0.44, 0.95)	0.11 (0.03, 0.30)	18 (6, 29)	1543
4	1.33 (1.24, 1.56)	0.04 (0.01, 0.22)	32 (1, 12)	989
5	1.38 (1.31, 1.60)	0.04 (0.01, 0.15)	2 (2, 6)	978

Table 2
Froude number, kinematic wave number, and non-dimensionalized period for Reaches 1–5. Data are provided for mean study period discharge, Q = 3 m^3/s (min discharge Q = 0.8 m^3/s, max discharge Q = 13 m^3/s).

Reach	Froude number, F_0	Kinematic wave number, k	Non-dimensionalized period, T+
1	0.05 (0.02, 0.12)	8814 (10825, 623)	86.24 (29.59, 179.42)
2	0.01 (0.06, 0.16)	806 (1573, 392)	116.25 (94.13, 123.86)
3	0.05 (0.02, 0.10)	1870 (833, 1881)	11.07 (1.45, 30.17)
4	0.02 (0.004, 0.06)	349 (585, 3778)	0.09 (0.03, 4.56)
5	0.01 (0.003, 0.04)	2772 (2452, 5149)	0.23 (0.05, 0.28)

58% to 8% and 7% using those same equations. On a reach-by-reach basis, the fit of in-situ data to Manning's equation with both constant and variable $\tilde{n}$ showed more consistent variation on the three upstream reaches than on the two reaches immediately above low-head dams for the in-situ data. For example, Reach 4 was characterized by relatively high error across all parameterizations of $\tilde{n}$ for the in-situ data, with an rRMSE for in-situ data that never fell below 23%, but uniformly low rRMSE for the modeled data, with rRMSE < 10% for all parameterizations. Conversely, Reach 5 had uniformly high error in the modeled data, where rRMSE never dropped below 59%, but rRMSE in the in-situ data dropped from 98% rRMSE to 19% rRMSE when parameterized with Eq. (9).

5. Discussion

The results of the hydraulic characterization support our use of the water surface slope in a modified Manning's equation. Observed kinematic wave numbers generally fell outside the range of values explored by both Vieira (1983) and Moussa and Bocquillon (1996), but these studies suggest a diffusive approximation is valid due to the low F_o (< 0.10) and very large k (> 15) values. The large T+ in Reaches 1 and 2 (T+ > 75) may indicate a kinematic regime is appropriate (Moussa and Bocquillon, 1996), but both the kinematic and diffusive approximations should be similar with low Froude and high kinematic wave numbers (Vieira, 1983), and the diffusive approximation is generally appropriate under low F_o conditions (F_o < 0.3) (Garambois and Monnier, 2015).

The observed increase in $\tilde{n}$ during low-flow conditions matched the increase reported by Durand et al. (2016) in both in-situ and modeled data, suggesting that the 'roughness' parameter may be better described as an effective resistance and that the primary source of this variation is a non-physical artifact of spatial averaging techniques. The in-situ data shows a non-linear decline of $\tilde{n}$ with both stage and discharge in both high-gradient and low-gradient reaches within the study area. This relationship also emerges from the modeled data when it is represented by reach-averaged values in the context of an open channel flow equation, despite the use of a constant roughness coefficient in the model run. The emergence of this relationship in reach-averaged calculations of both the in-situ and modelled data suggests that the observed variability in $\tilde{n}$ is largely an artifact of spatial averaging. In the case of the in-situ data, we cannot prove that Manning's equation held at cross sections with a constant roughness, but the presence of the same phenomenon in the modeled data provides a strong basis for our contention that the roughness variability observed in both datasets is an artifact of spatial averaging. Additional factors may be at play: since Manning's n is the only non-physical parameter in the equation, it may aggregate and compensate for other, unexplored sources of model error when fitting water surface data.

The observations in this paper do not provide a physical explanation for roughness variability in open channel flow, which is a well-documented phenomenon in the suite of Chezy-derived open channel flow equations (Yen, 2002). However, despite mention in the literature of the need to consider spatial variability (Li et al., 1992; Yen, 2002), many studies use reach-averaged hydraulic variables and report dynamic roughness coefficients without mention of the effects of spatial averaging. In real-world observations of fluvial hydraulics on relatively low-gradient rivers, this approach can be difficult to avoid; while channel shape can be measured at a discrete spatial location along a river, the energy grade or slope is a value measured over some continuous distance.

This variability in effective resistance has clear ramifications for discharge estimates derived from remote sensing data. For the forthcoming SWOT mission, obtaining accurate discharge estimates will rely on obtaining accurate measurements of water surface height, width, and slope. The mission's ability to meet its science requirements is conditional on the use of spatial averaging to reduce random noise in the data, requiring spatial averaging over reaches up to 10 km long (Desai, 2018). Such considerations of spatial averaging are not unique to SWOT; most remote measurements of water surface elevation, extent, and slope estimation intrinsically rely on some form of spatial averaging to reduce measurement error (Birkinshaw et al., 2014; Hall et al., 2012; O'Loughlin et al., 2013).

Also notable from the open-channel flow optimization results is the variation in error characteristics across river reaches. In both in-situ

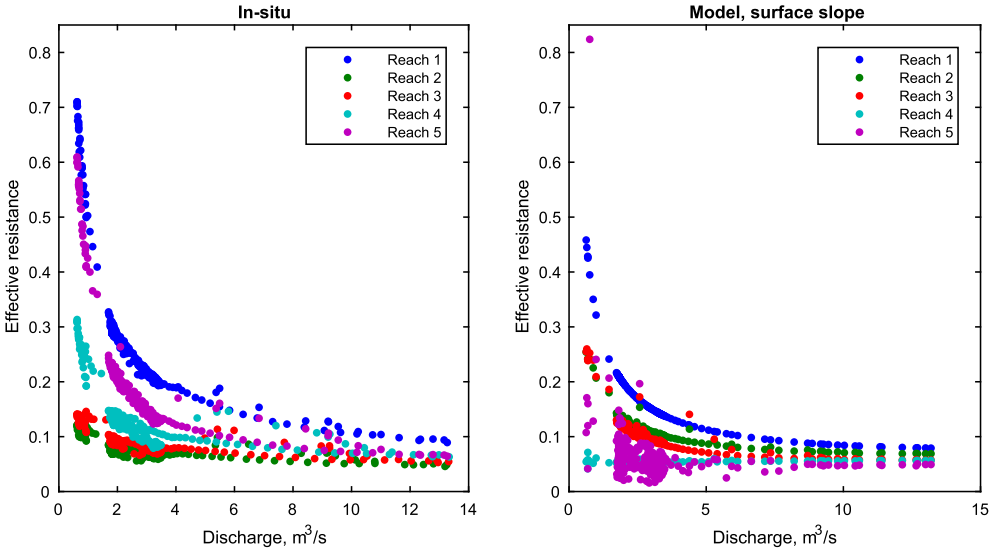

Fig. 7. Title: Back-calculated $\tilde{n}$ from in-situ and model output data. Caption: Comparison of reach-averages and results from using the water surface slope supplied by HEC-RAS.

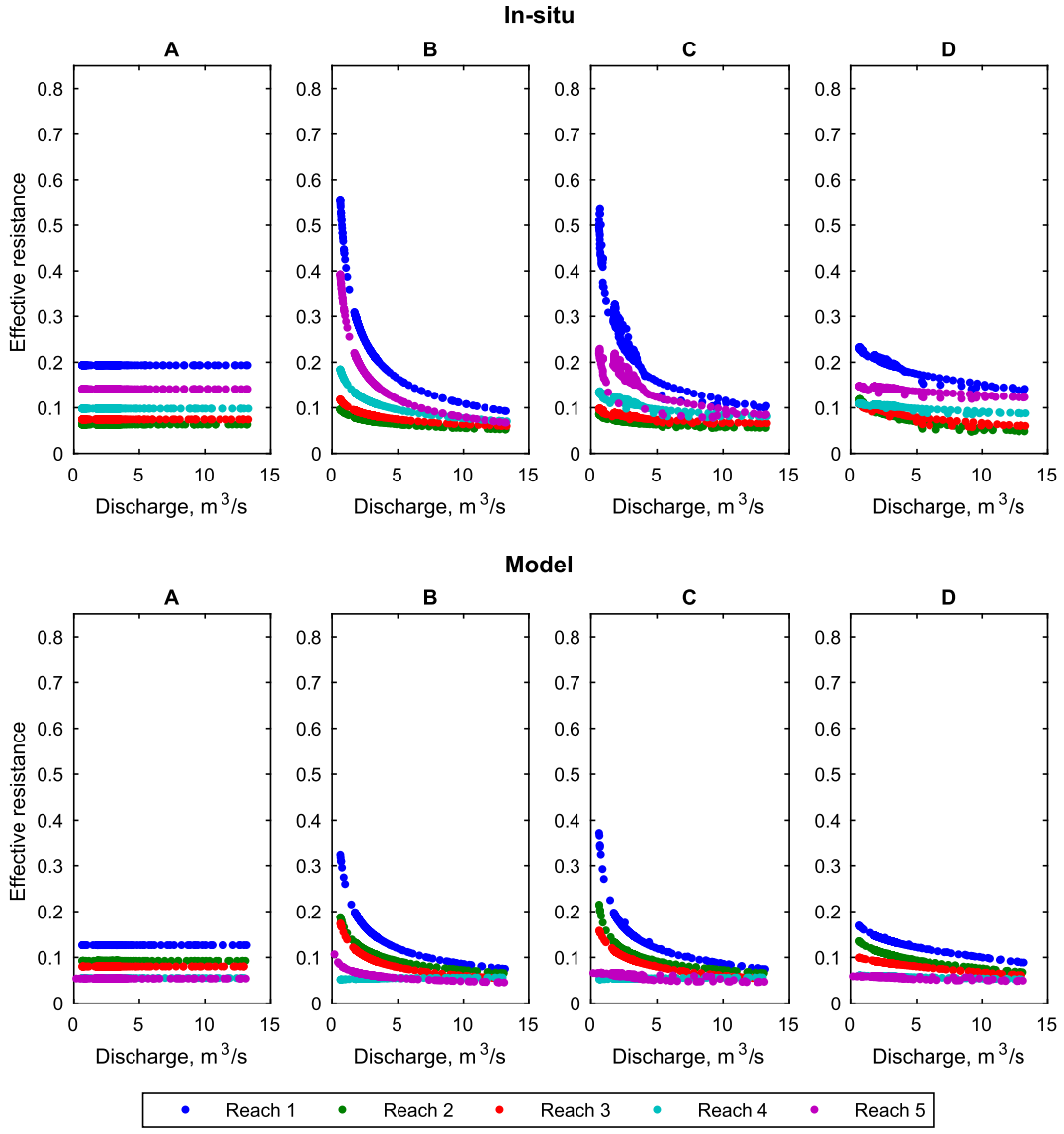

Fig. 8. Title: Effective resistance (ñ) estimated from in-situ and model output data. Caption: The formulations used to back-calculate ñ are as follows: (A) constant roughness (Eq. (8)), (B) power law relationship between resistance and stage (Eq. (9)), (C) power law relationship between resistance and discharge (Eq. (10)), and (D) logarithmic relationship between resistance and the depth of flow relative to bank full flow (Eq. (11)).

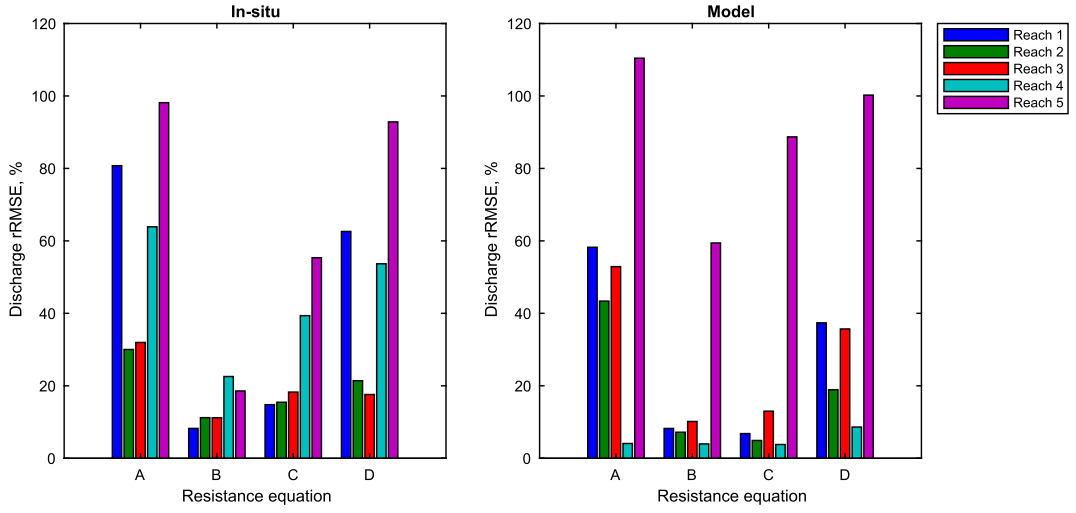

Fig. 9. Title: Relative root mean square errors for discharge estimated with Manning's equation using different ñ formulations. Caption: The formulations used in Manning's equation are as follows: (A) constant roughness (Eq. (8)), (B) power law relationship between resistance and stage (Eq. (9)), (C) power law relationship between resistance and discharge (Eq. (10)), and (D) logarithmic relationship between resistance and the depth of flow relative to bank full flow (Eq. (11)).

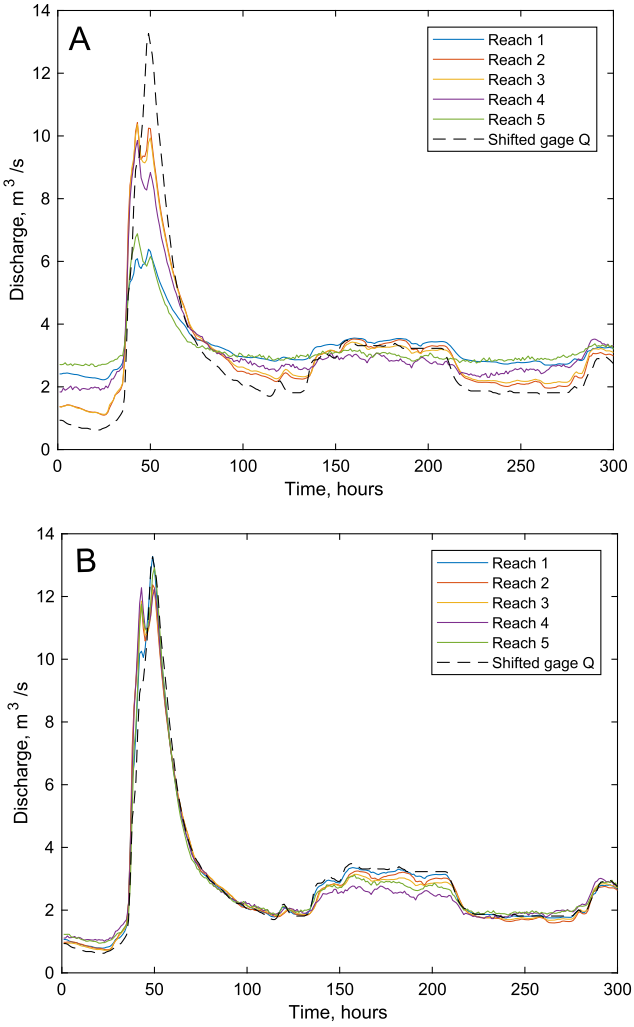

Fig. 10. Title: True and estimated discharge using constant (A) and variable (B) Manning's roughness. Caption: The top panel shows back-calculated discharge using a constant Manning's (Eq. (8)), while the bottom panel shows the same discharges calculated using a power law relationship between resistance and stage (Eq. (9)). The power-law roughness derived discharge captures the range of flows for all reaches and more closely approximates the true discharge than the constant roughness approach.

and modelled data, discharge errors were highest in one of the two furthest downstream reaches (Reaches 4 or 5), which were characterized by the largest cross sectional areas of flow, lowest average flow velocities, and smallest Froude number at mean flow. However, the 'worst' reach was not constant in the two cases: Reaches 4 and 5 had similarly large errors in the in-situ data, while errors were largest in Reach 5 in the model data. This may be due to instrument and model limitations; for Reaches 4 and 5, the low-head dams created very mild water surface slopes at low flow (< 5 cm/km), which are difficult to accurately resolve on a < 1 km reach using elevation constraints with $\sigma \approx 2$ cm in optimal circumstances; the model similarly showed a near-zero water surface slope at times. The contrast in errors between Reach 1 and Reaches 2 and 3 is also notable: the Manning's approximation with constant $\tilde{n}$ has much higher error on Reach 1 than Reaches 2 and 3, but the errors drop to very similar levels for all three reaches when a power law $\tilde{n}$ formulation is used. This disparity is possibly explained by a geomorphological issue: the first third (~ 500 m) of Reach 1 runs adjacent to a highway, where the channel is lined with rip-rap and characterized by series of artificial riffle-pool sequences with deep (> 1 m) pools. This flow regime contrasts sharply with the remaining 500 m of Reach 1 and with the entirety of Reaches 2 and 3, where the river flows in a shallow, meandering alluvial channel. These results suggest that the issue of spatial averaging in Manning's equation is affected by spatial variability at multiple scales, and that a couple of sharp hydraulic discontinuities can have outsized effects on variation in effective resistance.

While these results are merely observational, they do point to potential benefits of defining reaches with consistent hydraulic characteristics, and splitting reaches apart where the fundamental nature of the channel geomorphology changes (artificial to 'free-flowing', steep to mild, etc.). Frasson et al. (2017) presented automated reach definition methods that aim to create reaches with consistent hydraulic characteristics; however, the impact of reach definition on the variability of ñ has yet to be evaluated. In the broader SWOT context, our study reach represents a challenging, but relevant scenario: it is borderline SWOT observable (error statistics are given for a river of 100 m average width over a 10 km reach), but the issues associated with hydraulic discontinuities, river engineering, and lateral inflows are relevant to discharge estimates on many world rivers.

6. Conclusions

This study provides a novel perspective on the issue of roughness variability in Manning's equation by showing parallel roughness variability in both in-situ and modeled data. Creating a variable roughness parameterization in Manning's equation or other open channel flow formulations is not a novel concept, and both logarithmic and power-law formulations of roughness have been proposed with a more thorough physical or analytical basis than is provided here. However, this paper draws attention to the need to explicitly address spatial variability in roughness parameterizations, which is a problematic and under-discussed issue in applications of Manning's equation on natural rivers.

Given the results observed here, a two-parameter formulation of Manning's n to address contributors to flow resistance is appealing in the context of discharge estimates which use reach-averaged data products such as the suite of mass-conserved flow-law inversions proposed for SWOT discharge retrieval algorithms (Gleason et al., 2017). This approach adds complexity to both Manning's equation and those inversions, which would otherwise prescribe or solve for a singular flow resistance parameter for a given channel, and may contribute to further equifinality in algorithm solutions when three values – including two non-physical parameters – need to be found. Data assimilation approaches to remote sensing estimates of discharge may be able to use the full Saint Venant equations and bypass the issues discussed here, and have shown promising preliminary results (Oubanas et al., 2018a,b). However, we believe that there is potential and utility for these mass-conserved open-channel flow law inversions in the context of remote sensing due to their relatively low computational intensities and promising preliminary results (Durand et al., 2016; Hagemann et al., 2017; Yoon et al., 2016). Fully developing and promoting the idea of an 'effective resistance' parameterization (Li et al., 1992) in the context of discharge estimates from SWOT or other remote sensing missions will require further examination of these averaging effects and an analytical parameterization of induced roughness variability.

Declaration of Competing Interest

The authors declare that they have no known competing financial interests or personal relationships that could have appeared to influence the work reported in this paper.

Acknowledgements

This work was funded by NASA grants NNX13AD96G and NNX15AN33H.

Appendix A:. Constrained logger elevation estimator

The elevation of each logger on the river bed was calculated using water surface elevation measurements from GPS and depth data from the loggers. In order to minimize the errors in our estimated logger elevations while preserving the basic physics of the river system, we used a constrained estimator to calculate the logger elevation, Z, at all sites, ensuring that for all times and all sites, $Z_i + D_{i,t} > Z_{i+1} + D_{i+1,t}$, where D is the logger depth at site i and time t. The constrained estimator used a weighted objective function:

$$\|CZ - b\| \tag{A.1}$$

where C is a diagonal matrix of the inverse 3D coordinate quality (weight) and b is a vector of the weighted differences between measured logger depths and GPS measurements. Equation (A.1) was subject to a linear constraint at all time steps t at the native resolution of the logger data (5 min) and all loggers i:

$$AZ \leq b \tag{A.2}$$

where b is the difference in WSEs between successive loggers ($Z_i + D_i - Z_{i+1} + D_{i+1}$) and A is formulated such that $A_i < A_{i+1}$, where i is a logger and $i + 1$ is the next logger downstream.

Appendix B:. Algebraic reordering of Eq. (10)

Relating n back to Q as part of a power function leads to an interesting rewriting of Manning's equation. Starting with the equation for effective resistance, n:

$$n = aQ^b \tag{B.1}$$

and substituting into (1)

$$Q = \frac{1}{n}(\delta A + A_0)^{5/3} W^{-2/3} S^{1/2} \tag{B.2}$$

$$Q = \frac{1}{aQ^b}(\delta A + A_0)^{5/3} W^{-2/3} S^{1/2} \tag{B.3}$$

$$Q^{1+b} = \frac{1}{a}(\delta A + A_0)^{5/3} W^{-2/3} S^{1/2} \tag{B.4}$$

$$Q = \frac{1}{a}^{\frac{1}{1+b}} (\delta A + A_0)^{\frac{5}{3(1+b)}} W^{-\frac{2}{3(1+b)}} S^{\frac{1}{2(1+b)}} \tag{B.5}$$

This rearrangement suggests that the exponents on A, W, and S (or R and S in the traditional Manning's equation formulation) are affected by the reach averaging effect. In the in-situ results, the optimized b value varies from -1.11 to -0.03.

Appendix C:. Fit statistics for all height-width rating curves

Fit statistics for a linear regression of height-width relations for each of the twenty logger sites. Bolded rows show where $p < 0.05$ and we use the linear regression to calculate widths. Italicized rows show where $p < 0.05$ and a constant mean width was used. For Site 9, there were an insufficient number of measurements to complete a fit.

Site	Width/Stage slope	p-value	R^2
1	13.95	0.01	0.86
2	5.45	0.01	0.81
3	11.33	0.01	0.73
4	31.66	0.02	0.65
5	2.38	0.03	0.49
6	8.60	0.00	0.92
7	14.76	0.00	0.91
8	21.07	0.00	0.87
9	*N/A*	*N/A*	*N/A*
10	5.42	0.01	0.74
11	16.64	0.00	0.89
12	5.74	0.00	0.92
13	3.23	0.01	0.63
14	*−2.44*	*0.44*	*0.089*
15	4.51	0.01	0.88
16	*3.47*	*0.09*	*0.55*
17	*5.13*	*0.07*	*0.45*
18	2.42	0.02	0.99
19	*−0.34*	*0.92*	*0.0018*
20	*5.02*	*0.23*	*0.2305*

References

Alsdorf, D.E., et al., 2000. Interferometric radar measurements of water level changes on the Amazon flood plain. Nature 404, 174. https://doi.org/10.1038/35004560.

Alsdorf, D.E., Rodríguez, E., Lettenmaier, D.P., 2007. Measuring surface water from space. Rev. Geophys. 45 (2). https://doi.org/10.1029/2006rg000197.

Altenau, E.H., et al., 2017. AirSWOT measurements of river water surface elevation and slope: Tanana River, AK. Geophys. Res. Lett. 44 (1), 181–189. https://doi.org/10.1002/2016gl071577.

Asfaha, T.G., Frankl, A., Haile, M., Zenebe, A., Nyssen, J., 2015. Determinants of peak discharge in steep mountain catchments – Case of the Rift Valley escarpment of Northern Ethiopia. J. Hydrol. 529, 1725–1739. https://doi.org/10.1016/j.jhydrol.2015.08.013.

Bathurst, J.C., 1985. Flow resistance estimation in mountain rivers. J. Hydraul. Eng. 111 (4), 625–643. https://doi.org/10.1061/(ASCE)0733-9429(1985) 111:4(625).

Biancamaria, S., Lettenmaier, D.P., Pavelsky, T.M., 2016. The SWOT mission and its capabilities for land hydrology. Surv. Geophys. 37 (2), 307–337. https://doi.org/10.1007/s10712-015-9346-y.

Birkett, C.M., Mertes, L.A.K., Dunne, T., Costa, M.H., Jasinski, M.J., 2002. Surface water dynamics in the Amazon Basin: Application of satellite radar altimetry. J. Geophys. Res. Atmos. 107 (D20), LBA 26-1–LBA 26-21. https://doi.org/10.1029/2001jd000609.

Birkinshaw, S.J., et al., 2014. Daily discharge estimation at ungauged river sites using remote sensing. Hydrol. Process. 28 (3), 1043–1054. https://doi.org/10.1002/hyp.9647.

Bjerklie, D.M., et al., 2018. Satellite remote sensing estimation of river discharge: application to the Yukon River Alaska. J. Hydrol. 561, 1000–1018. https://doi.org/10.1016/j.jhydrol.2018.04.005.

Bjerklie, D.M., Moller, D., Smith, L.C., Dingman, S.L., 2005. Estimating discharge in rivers using remotely sensed hydraulic information. J. Hydrol. 309 (1–4), 191–209. https://doi.org/10.1016/j.jhydrol.2004.11.022.

Cardoso, A.H., Graf, W.H., Gust, G., 1989. Uniform flow in a smooth open channel. J. Hydraul. Res. 27 (5), 603–616. https://doi.org/10.1080/00221688909499113.

Chow, V., 1959. Open-Channel Hydraulics. Mc Graw-Hill, New Yourk, USA, pp. 700.

David, G.C.L., Wohl, E., Yochum, S.E., Bledsoe, B.P., 2011. Comparative analysis of bed resistance partitioning in high-gradient streams. Water Resour. Res. 47 (7). https://doi.org/10.1029/2010WR009540.

De Doncker, L., et al., 2009. Determination of the Manning roughness coefficient influenced by vegetation in the river Aa and Biebrza river. Environ. Fluid Mech. 9 (5), 549–567. https://doi.org/10.1007/s10652-009-9149-0.

Desai, S., 2018. Surface Water and Ocean Topography mission (SWOT), Science Requirements Document JPL document D-61923 Revision B, https://swot.jpl.nasa.gov/docs/D-61923_SRD_Rev_B_20181113.pdf, Jet Propulsion Laboratory, Retrieved March 3, 2019.

Dingman, S.L., 2009. Fluvial Hydraulics. Oxford University Press Inc, Oxford, pp. 570.

Durand, M., et al., 2016. An intercomparison of remote sensing river discharge estimation algorithms from measurements of river height, width, and slope. Water Resour. Res. 52, 4527–4549. https://doi.org/10.1002/2015wr018434.

Durand, M., et al., 2014. Estimating reach-averaged discharge for the River Severn from measurements of river water surface elevation and slope. J. Hydrol. 511, 92–104. https://doi.org/10.1016/j.jhydrol.2013.12.050.

Ferguson, R., 2007. Flow resistance equations for gravel- and boulder-bed streams. Water Resour. Res. 43 (5). https://doi.org/10.1029/2006WR005422.

Ferguson, R., 2010. Time to abandon the Manning equation? Earth Surf. Process. Landf. 35 (15), 1873–1876. https://doi.org/10.1002/esp.2091.

Ferguson, R.I., Sharma, B.P., Hardy, R.J., Hodge, R.A., Warburton, J., 2017. Flow resistance and hydraulic geometry in contrasting reaches of a bedrock channel. Water Resour. Res. 53 (3), 2278–2293. https://doi.org/10.1002/2016WR020233.

Frasson, R.P.D.M., et al., 2017. Automated river reach definition strategies: applications for the surface water and ocean topography mission. Water Resour. Res. 53 (10), 8164–8186. https://doi.org/10.1002/2017wr020887.

Froehlich, D.C., 2012. Resistance to shallow uniform flow in small, riprap-lined drainage channels. J. Irrig. Drain. Eng. 138 (2), 203–210. https://doi.org/10.1061/(ASCE)IR.1943-4774.0000383.

Garambois, P.A., Monnier, J., 2015. Inference of effective river properties from remotely sensed observations of water surface. Adv. Water Resour. 79, 103–120. https://doi.org/10.1016/j.advwatres.2015.02.007.

Gleason, C., Garambois, P.A., Durand, M.T., 2017. Tracking river flows from space. EOS 98. https://doi.org/10.1029/2017EO078085.

Gleason, C.J., Smith, L.C., 2014. Toward global mapping of river discharge using satellite images and at-many-stations hydraulic geometry. Proc. Natl. Acad. Sci. USA 111 (13), 4788–4791. https://doi.org/10.1073/pnas.1317606111.

Gleason, C.J., Smith, L.C., Lee, J., 2014. Retrieval of river discharge solely from satellite imagery and at-many-stations hydraulic geometry: Sensitivity to river form and optimization parameters. Water Resour. Res. 50 (12), 9604–9619. https://doi.org/10.1002/2014wr016109.

Hagemann, M.W., Gleason, C.J., Durand, M.T., 2017. BAM: Bayesian AMHG-manning inference of discharge using remotely sensed stream width, slope, and height. Water Resour. Res. 53 (11), 9692–9707. https://doi.org/10.1002/2017WR021626.

Hall, A.C., Schumann, G.J.-P., Bamber, J.L., Bates, P.D., Trigg, M.A., 2012. Geodetic corrections to Amazon River water level gauges using ICESat altimetry. Water Resour. Res. 48 (6). https://doi.org/10.1029/2011WR010895.

Harman, C., Stewardson, M., DeRose, R., 2008. Variability and uncertainty in reach bankfull hydraulic geometry. J. Hydrol. 351 (1), 13–25. https://doi.org/10.1016/j.jhydrol.2007.11.015.

Hundey, E.J., Ashmore, P.E., 2009. Length scale of braided river morphology. Water Resour. Res. 45 (8). https://doi.org/10.1029/2008WR007521.

LeFavour, G., Alsdorf, D., 2005. Water slope and discharge in the Amazon River estimated using the shuttle radar topography mission digital elevation model. Geophys. Res. Lett. 32 (17). https://doi.org/10.1029/2005gl023836.

Legleiter, C.J., Kyriakidis, P.C., 2008. Spatial prediction of river channel topography by kriging. Earth Surf. Process. Landf. 33 (6), 841–867. https://doi.org/10.1002/esp.1579.

Li, S.G., Venkataraman, L., McLaughlin, D., 1992. Stochastic theory for irregular stream modeling. Part I: flow resistance. J. Hydraul. Eng. 118 (8), 1079–1090. https://doi.org/10.1061/(ASCE)0733-9429(1992)118:8(1079).

Lumbroso, D., Gaume, E., 2012. Reducing the uncertainty in indirect estimates of extreme flash flood discharges. J. Hydrol. 414–415, 16–30. https://doi.org/10.1016/j.jhydrol.2011.08.048.

MacWilliams Jr., M.L., Wheaton, J.M., Pasternack, G.B., Street, R.L., Kitanidis, P.K., 2006. Flow convergence routing hypothesis for pool-riffle maintenance in alluvial rivers. Water Resour. Res. 42 (10). https://doi.org/10.1029/2005WR004391.

Moody, J.A., Troutman, B.M., 2002. Characterization of the spatial variability of channel morphology. Earth Surf. Process. Landf. 27 (12), 1251–1266. https://doi.org/10.1002/esp.403.

Moussa, R., Bocquillon, C., 1996. Criteria for the choice of flood-routing methods in natural channels. J. Hydrol. 186 (1), 1–30. https://doi.org/10.1016/S0022-1694(96)03045-4.

Navratil, O., Albert, M.B., 2010. Non-linearity of reach hydraulic geometry relations. J. Hydrol. 388 (3), 280–290. https://doi.org/10.1016/j.jhydrol.2010.05.007.

O'Loughlin, F., Trigg, M.A., Schumann, G.J.P., Bates, P.D., 2013. Hydraulic characterization of the middle reach of the Congo River. Water Resour. Res. 49 (8), 5059–5070. https://doi.org/10.1002/wrcr.20398.

Oubanas, H., et al., 2018a. Discharge estimation in ungauged basins through variational data assimilation: the potential of the SWOT mission. Water Resour. Res. https://doi.org/10.1002/2017WR021735.

Oubanas, H., Gejadze, I., Malaterre, P.-O., Mercier, F., 2018b. River discharge estimation from synthetic SWOT-type observations using variational data assimilation and the full Saint-Venant hydraulic model. J. Hydrol. 559, 638–647. https://doi.org/10.1016/j.jhydrol.2018.02.004.

Papa, F., et al., 2010. Interannual variability of surface water extent at the global scale, 1993–2004. J. Geophys. Res. 115 (D12). https://doi.org/10.1029/2009JD012674.

Pavelsky, T.M., et al., 2014. Assessing the potential global extent of SWOT river discharge observations. J. Hydrol. 519, 1516–1525. https://doi.org/10.1016/j.jhydrol.2014.08.044.

Pavelsky, T.M., Smith, L.C., 2008. RivWidth: a software tool for the calculation of river widths from remotely sensed imagery. IEEE Geosci. Remote Sens. Lett. 5 (1), 70–73. https://doi.org/10.1109/lgrs.2007.908305.

Pekel, J.F., et al., 2016. High-resolution mapping of global surface water and its long-term changes. Nature 540 (7633), 418.

Powell, D.M., 2014. Flow resistance in gravel-bed rivers: Progress in research. Earth Sci. Rev. 136, 301–338. https://doi.org/10.1016/j.earscirev.2014.06.001.

Ringley, B.F., 2006. The Lower Olentangy River Watershed Lowhead Dams Feasibility Study, World Environmental and Water Resource Congress 2006, Omaha, Nebraska, pp. 1-12. DOI:10.1061/40856(200)190.

Rouse, H., 1943. Evaluation of boundary roughness, Proceedings of the 2nd Hydraulics Conference. University of Iowa, Iowa City, IA, pp. 105-116.

Smith, L.C., Isacks, B.L., Bloom, A.L., Murray, A.B., 1996. Estimation of discharge from three braided rivers using synthetic aperture radar satellite imagery: Potential application to ungaged basins. Water Resour. Res. 32 (7), 2021–2034. https://doi.org/10.1029/96wr00752.

Strelkoff, T.S., Clemmens, A.J., 2000. Approximating wetted perimeter in power-law cross section. J. Irrig. Drain. Eng. 126 (2), 98–109. https://doi.org/10.1061/(ASCE)0733-9437(2000) 126:2(98).

Sturm, T.W., 2001. Open Channel Hydraulics. McGraw-Hill, New York, pp. 492.

Tourian, M.J., Schwatke, C., Sneeuw, N., 2017. River discharge estimation at daily resolution from satellite altimetry over an entire river basin. J. Hydrol. 546, 230–247. https://doi.org/10.1016/j.jhydrol.2017.01.009.

Trigg, M.A., et al., 2009. Amazon flood wave hydraulics. J. Hydrol. 374 (1–2), 92–105. https://doi.org/10.1016/j.jhydrol.2009.06.004.

U.S. Geological Survey, 2000. HYDRO1k Elevation Derivative Database. Cent. for Earth Resour. Obs. and Sci., Sioux Falls, S. D. doi: 10.5066/F77P8WN0 Retrieved from www.usgs.gov/centers/eros/science/usgs-eros-archive-digital-elevation-hydro1k.

Vieira, J.H.D., 1983. Conditions governing the use of approximations for the Saint-Vénant equations for shallow surface water flow. J. Hydrol. 60 (1), 43–58. https://doi.org/10.1016/0022-1694(83)90013-6.

Wallis, S.G., Knight, D.W., 1984. Calibration studies concerning a one-dimensional numerical tidal model with particular reference to resistance coefficients. Estuar. Coast. Shelf Sci. 19 (5), 541–562. https://doi.org/10.1016/0272-7714(84)90015-5.

Yen, B.C., 2002. Open Channel Flow Resistance. J. Hydraul. Eng. 128 (1), 20–39. https://doi.org/10.1061/(ASCE)0733-9429(2002) 128:1(20).

Yochum, S.E., Bledsoe, B.P., David, G.C.L., Wohl, E., 2012. Velocity prediction in high-gradient channels. J. Hydrol. 424–425, 84–98. https://doi.org/10.1016/j.jhydrol.2011.12.031.

Yoon, Y., et al., 2016. Improved error estimates of a discharge algorithm for remotely sensed river measurements: Test cases on Sacramento and Garonne Rivers. Water Resour. Res. 52 (1), 278–294. https://doi.org/10.1002/2015wr017319.